NANO LETTERS

Letter

pubs.acs.org/NanoLett

Phonon-Assisted Ultrafast Charge Transfer at van der Waals Heterostructure Interface

Qijing Zheng,[†] Wissam A. Saidi,[‡] Yu Xie,[§,∥] Zhenggang Lan,[§,∥] Oleg V. Prezhdo,[⊥] Hrvoje Petek,[#] and Jin Zhao*[,†,#,∇]

[†]ICQD/Hefei National Laboratory for Physical Sciences at Microscale, and Key Laboratory of Strongly-Coupled Quantum Matter Physics, Chinese Academy of Sciences, and Department of Physics, University of Science and Technology of China, Hefei, Anhui 230026, China

[‡]Department of Mechanical Engineering and Materials Science, University of Pittsburgh, Pittsburgh, Pennsylvania 15261, United States

[§]Key Laboratory of Biobased Materials, Qingdao Institute of Bioenergy and Bioprocess Technology, Chinese Academy of Sciences, Qingdao, Shandong 266101, China

[∥]University of Chinese Academy of Sciences, Beijing 100049, China

[⊥]Departments of Chemistry, and Physics and Astronomy, University of Southern California, Los Angeles, California 90089, United States

[#]Department of Physics and Astronomy, University of Pittsburgh, Pittsburgh Pennsylvania 15260, United States

[∇]Synergetic Innovation Center of Quantum Information & Quantum Physics, University of Science and Technology of China, Hefei, Anhui 230026, China

Supporting Information

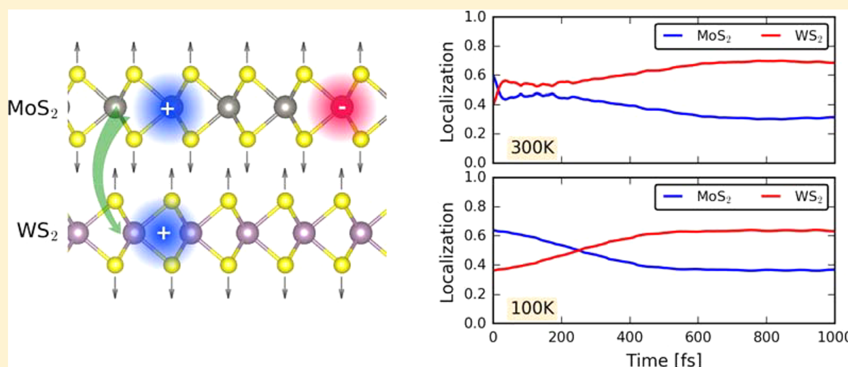

ABSTRACT: The van der Waals (vdW) interfaces of two-dimensional (2D) semiconductor are central to new device concepts and emerging technologies in light-electricity transduction where the efficient charge separation is a key factor. Contrary to general expectation, efficient electron−hole separation can occur in vertically stacked transition-metal dichalcogenide heterostructure bilayers through ultrafast charge transfer between the neighboring layers despite their weak vdW bonding. In this report, we show by *ab initio* nonadiabatic molecular dynamics calculations, that instead of direct tunneling, the ultrafast interlayer hole transfer is strongly promoted by an adiabatic mechanism through phonon excitation occurring on 20 fs, which is in good agreement with the experiment. The atomic level picture of the phonon-assisted ultrafast mechanism revealed in our study is valuable both for the fundamental understanding of ultrafast charge carrier dynamics at vdW heterointerfaces as well as for the design of novel quasi-2D devices for optoelectronic and photovoltaic applications.

KEYWORDS: *van der Waals heterointerface, nonadiabatic molecular dynamics, ultrafast charge transfer*

Van der Waals (vdW) heterostructures are a new class of two-dimensional (2D) materials with special optical and electronic properties.[1−16] Among these newly created materials, the transition-metal dichalcogenide (TMD) heterostructures are particularly interesting for optoelectronics and solar energy conversion[5,10,14−20] because their optical band gaps are in the visible spectral region and light−matter interactions are strong.[19−24]

Efficient charge separation is a key factor for optoelectronics and solar energy conversion, which can be accomplished by fast

Received: August 10, 2017
Published: September 15, 2017

Downloaded via UNIV SCIENCE AND TECHNOLOGY CHINA on October 13, 2021 at 11:32:19 (UTC).
See https://pubs.acs.org/sharingguidelines for options on how to legitimately share published articles.

ACS Publications © 2017 American Chemical Society

DOI: 10.1021/acs.nanolett.7b03429
Nano Lett. 2017, 17, 6435−6442

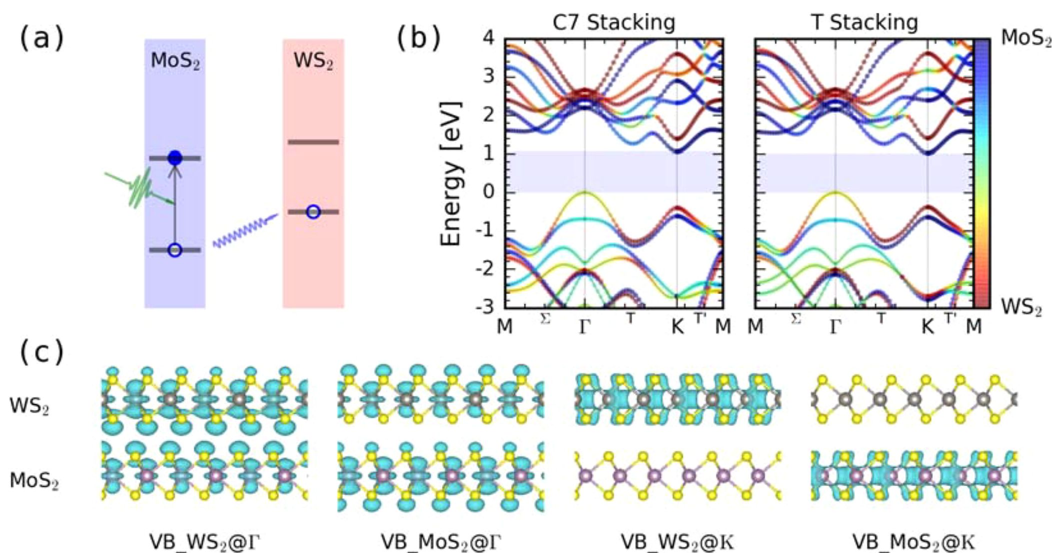

Figure 1. Band structures and orbital spatial distributions of a MoS_2/WS_2 heterostructure with C7 and T stackings. (a) Schematic of the photoexcitation and hole transfer in a MoS_2/WS_2 heterostructure. (b,c) Band structures (C7 and T stackings) and orbital spatial distributions (C7 stacking) of VB states of the MoS_2/WS_2 heterostructure calculated by DFT. The momentum-dependent hole localization for different bands is indicated by their coloring according to the color strip in (b).

interlayer charge transfer. Most vertically stacked TMD heterostructures show type II band alignment where the conduction band minimum (CBM) and the valence band maximum (VBM) reside on different layers.[25−29] This feature facilitates the electron−hole separation after a photoexcitation and consequently increases the photocarrier lifetime. However, the weak vdW interaction and strong interaction in single layer TMD are expected to inhibit interlayer charge transfer in the TMDs.[22,23,30−32]

Contrary to these expectations, ultrafast interlayer charge transfer has been experimentally observed in TMD heterostructures.[5,6,33,34] Among the experimental observations, the shortest time scale was obtained in ultrafast measurements on MoS_2/WS_2 heterostructures by Hong et al. in which they found that the holes transfer from MoS_2 to WS_2 layer with an upper limit of 50 fs. Such surprisingly fast interlayer charge-transfer time scales have not been reconciled with the predominantly weak physical-coupling between the layers.

In this report, we employ time-dependent *ab initio* nonadiabatic molecular dynamics (NAMD) to elucidate the fundamental aspects of the ultrafast hole dynamics at vdW heterostructure interface with type II band alignment. We focus on the hole dynamics in MoS_2/WS_2 schematically shown in Figure 1a. Our results reveal that the ultrafast interlayer hole transfer is not mediated by the nonadiabatic (NA) charge tunneling mechanism; but instead, it is facilitated by an AD process, which is promoted by specific phonons and occurs within 20 fs. The phonon-assisted ultrafast mechanism revealed in our study gives atomic level insights into the ultrafast charge transfer occurring at vdW heterostructure interfaces, which are valuable both for the fundamental understanding and the design of novel quasi-2D devices for optoelectronic and photovoltaic applications.

The *ab inito* NAMD calculations are implemented within time domain density functional theory (TDDFT). The simulations are carried out using the Vienna *ab initio* simulation package (VASP)[35−37] augmented with the NAMD capabilities.[38,39] The generalized gradient approximation functional of PBE[40] and the projector augmented wave (PAW)[41] approximation for the core electrons are used. The sufficiency of PBE functional is discussed in the Supporting Information by comparing with HSE functional and previous GW calculations. vdW interactions are included in the simulations using the D2 approach,[42] which qualitatively agrees with the vdW-DF method using the optB86b functional. (See Supporting Information for more details.) The MoS_2/WS_2 heterostructure is modeled using an orthogonal 3×3 supercell with 108 atoms sampled at the Γ point. Because of the large supercells, seven irreducible K points including the Γ and K points of the primitive unit cell are included and can be assigned by unfolding the energy bands (see the Supporting Information).

We investigate two different stackings, C7 and T, which have the lowest energies.[29] The geometric structures are shown in the Supporting Information. After the geometry optimization, we use velocity rescaling to bring the temperature of the system to either 100 or 300 K, a 5 ps microcanonical *ab initio* molecular dynamics trajectory is then generated with a time step of 1 fs. Using the molecular dynamics trajectory, the NAMD results are based on averaging over 100 different initial configurations. For each chosen structure, we sample 2×10^4 trajectories for the last 2 ps.[43−45] More details about the simulations can be found in the Supporting Information.

Before describing the NAMD results, it is informative to inspect the band structure. First, the band structures for C7 and T stackings are nearly identical. Second, the calculation confirms that the MoS_2/WS_2 heterostructure has a type II band alignment where the CBM and VBM reside on MoS_2 and WS_2, respectively. Third, the orbital hybridization varies significantly with the momentum within a band, as can be seen from the color map in Figure 1b and the corresponding orbital distributions in Figure 1c. For example, at the K point, the interlayer hybridization is weak. By contrast, at the Γ point, the hybridization is stronger, and consequently the orbitals are delocalized over both layers. Because of the relatively strong interlayer hybridization with antibonding character at the Γ point, VBM of MoS_2/WS_2 residing on WS_2 at K point is around 0.2 eV higher than the corresponding VB on WS_2. Overall, our band structures are consistent with previous studies.[25−29]

DOI: 10.1021/acs.nanolett.7b03429
Nano Lett. 2017, 17, 6435−6442

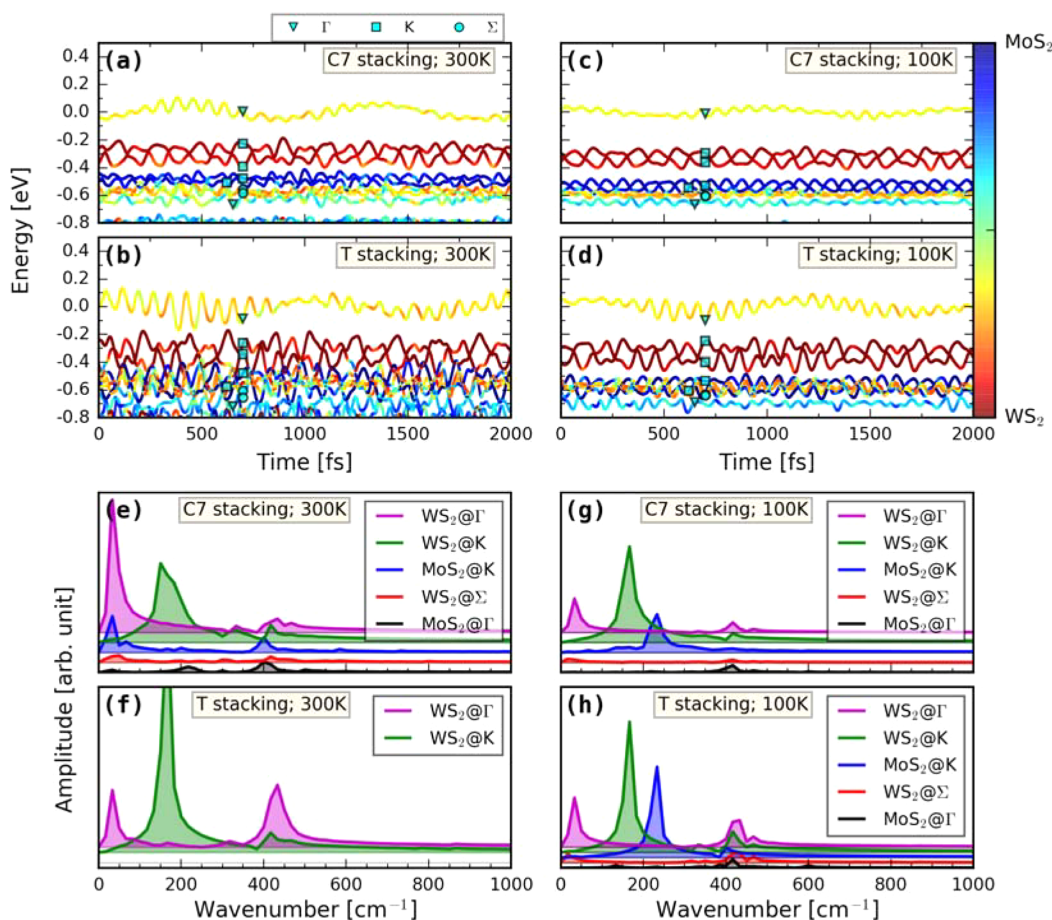

Figure 2. Time evolutions of the energy states near VBM (a−d) and their FT spectrum (e−h) for C7 and T stackings at 300 and 100 K. The energy reference in panels a−d is the average VBM energy, and the color map shows the hole localization. The triangle, square, and circle in panels a−d indicate the momentum of different energy states.

Before the interlayer charge transfer happens, the photoexcitation initially generates intralayer excitons. Besides the direct (K−K) exciton, it has been proposed that the indirect (Γ−K) exciton can also be formed through the intervalley scattering.[46−50] Therefore, the hole transfer from MoS_2 to WS_2 could happen at either the K or Γ point, and we investigate the hole dynamics associated with each point.

Time-dependent energy evolutions of the states near VBM for the C7 and T stackings are shown in Figure 2a,b. Here we use the same color map as in Figure 1b to show the orbital localization. For C7 stacking (Figure 2a), the VBM (WS_2@Γ) energy, shown by a light-red line, oscillates with amplitude of 0.1 eV during the MD trajectory. For lower energies, in the range of [−0.4, −0.2] eV, the two deep red lines represent the VB states at K on WS_2 (WS_2@K). In the energy range, around [−0.5, −0.4] eV, there are two deep blue lines representing VB states at K on MoS_2 (MoS_2@K). Below them in the energy range of [−0.7, −0.5] eV, there are three strongly hybridized states: the two light-red lines represent the two VB states on WS_2 for momentum 1/3 midway from Γ to M (WS_2@Σ), and one light-blue line represents the VB states on MoS_2 at Γ (MoS_2@Γ). Time-dependent energy evolution for the T stacking (Figure 2b) does not show significant difference except the larger oscillation amplitude. This can be induced by different e−p couplings and initial phonon excitation.

Time-dependent hole population transfer between two layers can be obtained from NAMD calculations by projecting the hole localization onto the MoS_2 and WS_2 layers, as shown in Figure 3. Moreover, the time-dependent hole-energy change can also be deduced by evaluating the hole probability distribution for selected energy states from the NAMD, as shown in Figure 4. By comparing Figures 3 and 4, the hole relaxation route in both real and momentum spaces can be obtained. We first investigate hole dynamics at the K point as shown in Figure 3a,b in which the initial hole is placed at MoS_2@K. Very interesting hole relaxation is found for the T stacking (Figure 3b) in which the charge transfer occurs on both fast and slow time scales. The fast component corresponds to a hole transfer from MoS_2 to WS_2 within $\tau_1 \approx 20$ fs, whereby the hole distribution on WS_2 increases from 10% to 55%. After the primary transfer is completed, the slow component involves an intralayer hole relaxation with $\tau_2 \approx 600$ fs time scale, whereby the hole distribution on WS_2 converges to 70%. The time-dependent hole-energy change shown in Figure 4b indicates that within the first 300 fs, most of the hole is distributed around −0.5 eV, corresponding to MoS_2@K and WS_2@Σ states. Therefore, we believe that the ultrafast interlayer hole transfer takes place between MoS_2@K and WS_2@Σ states ($\tau_1 \approx 20$ fs). After 600 fs, from Figure 4b, we see a distinct increase at 0 eV (WS_2@Γ state), which suggests that most of the hole relaxes from WS_2@Σ to WS_2@Γ (VBM) in $\tau_2 \approx 600$ fs within the VB of WS_2. We can assign the major hole transfer route to be MoS_2@K−WS_2@Σ−WS_2@Γ as shown in Figure 3b, in which MoS_2@K−WS_2@Σ corresponds to the

DOI: 10.1021/acs.nanolett.7b03429
Nano Lett. 2017, 17, 6435−6442

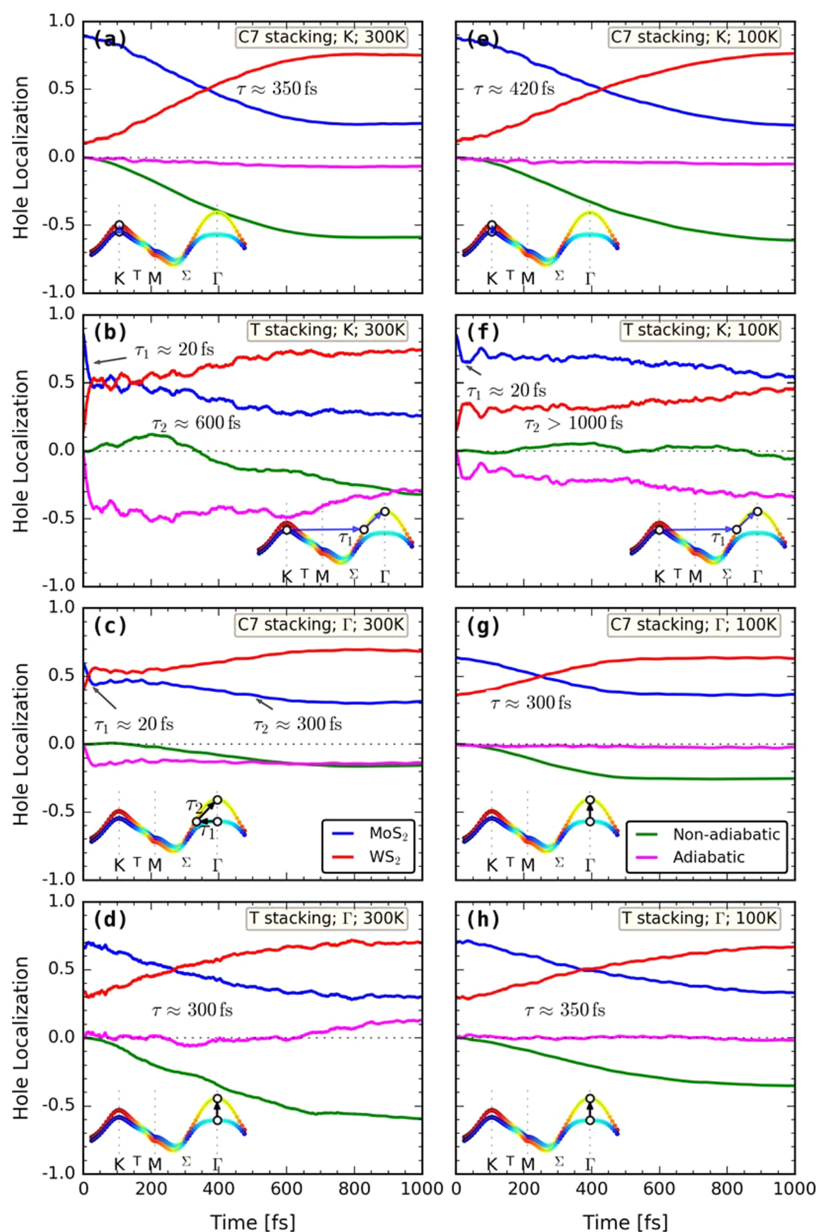

Figure 3. Time-dependent spatial hole localization at the K and Γ points for the C7 and T stackings at 300 K [K point (a,b), Γ point (c,d)] and 100 K [K point (e,f), Γ point (g,h)]. The major hole relaxation routes in momentum space are schematically shown in the insets. The AD and NA contributions to the hole dynamics are shown, where their sum indicates the decrease of hole localization within the MoS_2 layer.

ultrafast component. There is also a small portion of hole transfer through MoS_2@K−WS_2@K−WS_2@Γ without ultrafast component. In contrast, the ultrafast interlayer hole transfer is not found for the C7 stacking. The hole transfer happens in 300 fs, directly from MoS_2@K to WS_2@K, as shown in Figure 3a.

The hole transfer dynamics at Γ point is also investigated. Interestingly, in this case, the ultrafast interlayer charge transfer is found in C7 stacking, where the charge transfer occurs on both fast and slow time scales (Figure 3c). The fast interlayer transfer component happens within $\tau_1 \approx 20$ fs, with the hole distribution on WS_2 increasing from 40% to 60%. The following slow intralayer hole relaxation occurs in $\tau_2 \approx 300$ fs, whereby the hole distribution on WS_2 converges to 70%. By comparing with the time-dependent hole-energy change shown in Figure 4c, we can assign the major hole transfer route to be MoS_2@Γ−WS_2@Σ−WS_2@Γ in which MoS_2@Γ−WS_2@Σ corresponds to the ultrafast component. At the Γ point, the ultrafast interlayer hole transfer is not observed for the T stacking. The interlayer hole transfer takes place around 300 fs (Figure 3d) following the route of MoS_2@Γ−WS_2@Γ.

The AD and NA mechanisms compete in the hole relaxation. During a molecular dynamics trajectory, AD charge-transfer is provoked by nuclear motion, where transfer probability increases as the nuclear motion causes energy states to cross. By contrast, NA charge-transfer involves direct charge hopping or tunneling between different states. These two mechanisms can be distinguished as described in the Supporting Information. In Figure 3a−d, we show separately the AD and NA contributions to the hole dynamics at 300 K. One can see that for both the C7 and T stackings, the ultrafast interlayer hole transfer process ($\tau_1 \approx 20$ fs) is dominated by the AD charge transfer mechanism. This can be explained by the sufficiently close energy between the donor (MoS_2@K in T and MoS_2@Γ in C7 stacking) and acceptor (WS_2@Σ) states along

DOI: 10.1021/acs.nanolett.7b03429
Nano Lett. 2017, 17, 6435−6442

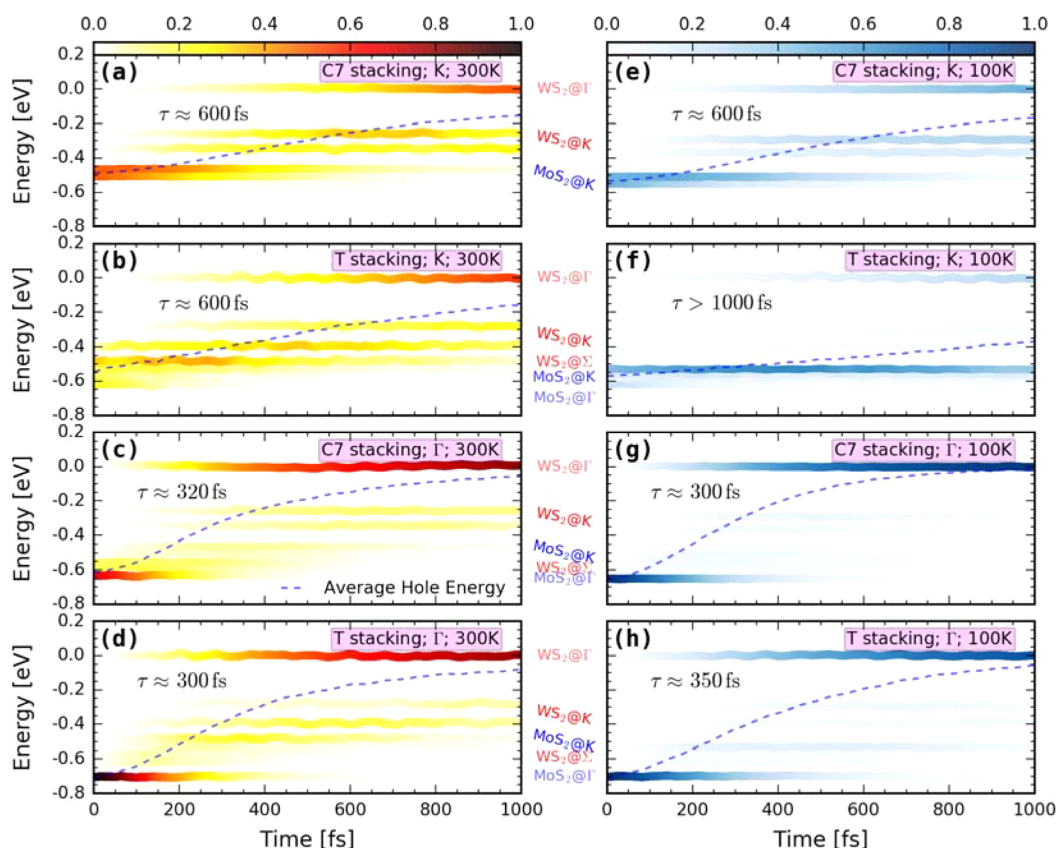

Figure 4. Time-dependent hole energy change at the K and Γ points for the C7 and T stacking at 300 K [K point (a,b), Γ point (c,d)] and 100 K [K point (e,f), Γ point (g,h)]. The color strips indicate the hole distribution on different energy states, and the dashed line represents the averaged hole energy. The energy reference is the average VBM energy.

with many crossings between them during an MD path. By contrast, the slow interlayer hole transfer process (Figure 3a,d) is almost completely promoted by the NA charge transfer mechanism.

Because the ultrafast interlayer hole transfer is provoked by the AD mechanism, we expect that this process is strongly sensitive to phonon excitation. To verify this, we perform additional NAMD calculations at a lower temperature of 100 K, which is expected to reduce the phonon occupation and therefore the oscillation amplitude. The decrease of vibrational amplitude is clearly seen in the plot of time-dependent energy of states near VBM in Figure 2c,d. Because of the decreased nuclear motion, there are almost no crossings between the donor (MoS_2@Γ in C7 and MoS_2@K in T stacking) and acceptor (WS_2@Σ) states.

Figures 3e,f and 4e,f show the time-dependent hole population transfer between two layers and hole energy change at 100 K. It is evident that cooling the sample suppresses the ultrafast hole transfer component for both the C7 and T stackings. For the C7 stacking the hole charge rearrangements consist solely of the direct hole hopping from MoS_2@Γ to WS_2@Γ on a time scale of around 300 fs, which are driven by the NA coupling, namely, direct charge tunneling. In the T stacking, the ultrafast hole transfer is not completely suppressed; however, the hole distribution on WS_2 only increases from 10% to 30% within the first 20 fs and then is followed by slow hole dynamics longer than 1 ps. By contrast, for the slow hole transfer processes the hole dynamics are essentially the same as at 300 K, as shown in Figure 3e,h, which is consistent with the predominantly NA coupling at both temperatures.

The temperature-dependent investigations clearly show that the ultrafast interfacial charge transfer from MoS_2@Γ/MoS_2@K to WS_2@Σ is assisted by the phonons and thus is expected to diminish at low temperatures. The vibrational modes of phonons, which couple to electronic states can be obtained by Fourier transforms (FTs) of the time-dependent state energy evolutions, as shown in Figure 2e,h. We interpret the FT frequencies by comparing them with the literature values.[51−53] Our results show that the donor (MoS_2@Γ/MoS_2@K) and acceptor (WS_2@Σ) states are coupled to the intralayer out-of-plane A_1 optical phonon at ∼400 cm^{-1}, a LA mode at ∼200 cm^{-1}, and the optical out-of-plane interlayer breathing mode at ∼35 cm^{-1}. These phonons have corresponding vibrational periods of 83, 166, and 953 fs. The ultrafast component of 20 fs is approximately one-quarter cycle of the A_1 mode with the period of 83 fs, suggesting that A_1 mode is the most important one for promoting the ultrafast charge transfer. The optical interlayer breathing mode with much longer vibrational period has little contribution to the ultrafast hole transfer. The phonon assisted hole transfer process is analogous to the anti-Stokes process. At 100 K, the hole transfer is dominated by NA charge transfer, which happens at ∼300−400 fs. At 300 K, the phonons have been absorbed, and the AD charge transfer channel is activated. Thus, the interlayer charge transfer happens within 20 fs. For such phonon-assisted charge transfer, the phonon excitation, e−p coupling matrix elements, and the energy difference between the donor−acceptor states are key factors that can influence the phonon-assisted charge transfer.

We notice that the significant temperature effect was not observed in the experiments.[5] This is mainly due to the

DOI: 10.1021/acs.nanolett.7b03429
Nano Lett. 2017, 17, 6435−6442

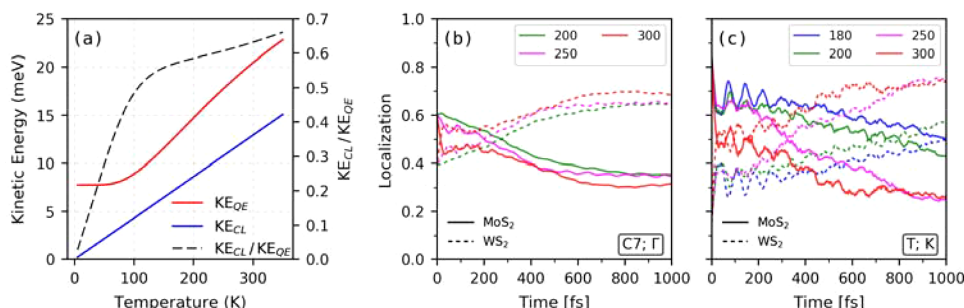

Figure 5. (a) Temperature dependence of KE_{QE} and KE_{CL}. The ratio KE_{CL}/KE_{QE} is also plotted. (b,c) Time-dependent spatial hole localization at different temperatures (300, 250, and 200 K for C7 stacking at Γ point (b), and 300, 250, 200, and 180 K for T stacking at K point (c)].

quantum nuclear effects, which are neglected in our NAMD simulations in which the nuclear motion is treated classically. To account for the quantum nuclear effects, we develop and implement the following model. Based on the FFT spectra shown in Figure 2e−h, one can estimate an averaged phonon frequency by $\bar{\varpi} = \sum_i \varpi_i I_i / \sum_i I_i$, where I is the intensity of the FFT phonon peak corresponding to the ith phonon mode. Note that all spectra are dominated by one or two intense signals, justifying our use of the averaged frequency. For both C7 and T stacking, the averaged phonon frequency at both 300 and 100 K can be estimated to be $\bar{\varpi} \approx 250$ cm^{-1}. Then, the quantum kinetic energy (KE) of the phonon system can be estimated as half of the total energy, which can be written using Bose−Einstein statistics as

$$KE_{QE} \approx \left(\frac{\hbar\bar{\varpi}}{2} + \frac{\hbar\bar{\varpi}}{\exp(\hbar\bar{\varpi}/K_B T) - 1} \right) / 2$$

In contrast, the classical kinetic energy can be estimated as

$$KE_{CL} \approx K_B T/2$$

In Figure 5a we plot out KE_{QE} and KE_{CL} and their ratio KE_{CL}/KE_{QE}. One can see that the change of KE_{CL}/KE_{QE} has a turning point between 100−150 K, suggesting that below 100 K the nuclear quantum effects increase distinctly. It can be seen that KE_{QE} (T = 100 K) ≈ KE_{CL} (T = 210 K), suggesting that to simulate an experimental measurement at 100 K, one needs to perform a simulation at around 210 K. Further, KE_{QE} (T = 0 K) ≈ KE_{CL} (T = 180 K), implying the existence of zero-point energy. It suggests that a temperature of 180 K is still needed to simulate the measurement at 0 K.

To make a better comparison with experimental results, we performed more detailed temperature-dependent simulations for C7 and T stackings at 300, 250, 200, and 180 K. The results are shown in Figure 5b,c. The details can be found in the Supporting Information. For C7 stacking, the phonon-assisted ultrafast charge transfer happens at 300 and 250 K, but disappear at 200 K, suggesting the critical temperature for ultrafast hole transfer is within 200−250 K range in the classical regime; the corresponding temperature falls in 90−135 K range if quantum nuclear effects are included. For T stacking, the ultrafast process still happens when the temperature is decreased to 180 K, implying that such an ultrafast process can be observed even near zero temperature. By considering the quantum nuclear effects, our model and simulations explain the ultrafast hole transfer at 80 K observed in the experiments.[5]

The phonon-assisted ultrafast charge transfer is found for both the C7 and T stackings: in both cases, the ultrafast charge transfer happens through the MoS_2@Γ−WS_2@Σ and MoS_2@K−WS_2@Σ pathways because energy differences between the donors and acceptors are sufficiently small. Actually, the three states of MoS_2@Γ, MoS_2@K, and WS_2@Σ are located within 0.1 eV, and thus, the phonon-assisted charge transfer can happen through either the Γ or the K point. The exact charge transfer route could depend on the respective stacking structure and other environmental factors. To confirm the independence of the ultrafast charge transfer on stacking, we have tested the least stable stacking, AA (see the Supporting Information), in which the ultrafast hole transfer of 20 fs is also obtained. For the AA stacking, which has the weakest interlayer interaction, a lateral interlayer shifting is observed in the MD process. However, this interlayer shifting does not influence the ultrafast interlayer hole transfer. The stacking independent results are in good agreement with the experiments.[5,6,34,54]

Alongside the experiments, there have been two recent theoretical publications, which also discussed the ultrafast hole dynamics at TMD vdW heterostructure interfaces. The work by Long et al. investigated the charge transfer from MoS_2 to $MoSe_2$ using a method similar to ours.[55] However, instead of choosing a hole donor state localized at MoS_2, they chose the highly delocalized $MoSe_2$@Γ state as a donor state; what they actually found is an intralayer relaxation from $MoSe_2$@Γ to $MoSe_2$@K, which does not address interlayer charge transfer as in our case. Wang et al. investigated the hole transfer from MoS_2 to WS_2 using TDDFT based on the Ehrenfest approximation,[56] which is different from our surface hopping scheme.[57−59] In addition, the supercell that they used does not include the Σ point in the Brillouin zone, and thus, the hole acceptor state WS_2@Σ is missing. That may explain why they failed to find the ultrafast interlayer hole transfer.

To conclude, our results show that the charge transfer through the NA (direct tunneling) mechanism is much slower than the phonon-assisted AD process at vdW interfaces with weak bonding. In MoS_2/WS_2, if phonon amplitudes are reduced, the interlayer hole transfer by direct tunneling (NA mechanism) takes about 300 fs even at the Γ point, which has a relatively strong interlayer orbital hybridization; this is much slower than the experimentally observed one transfer time.[5,6,33,34] Therefore, the calculated phonon-assisted (AD) charge transfer mechanism is essential to explain the 50 fs time scale charge transfer found in experiments.[5] Finally, involvement of small molecules at the interface is not completely ruled out as an additional charge transfer pathway. Furthermore, we are not able to include excitonic effects in our NAMD calculations. We believe that the interfacial charge transfer can take place even if the exciton binding energy is large as is the case in 2D TMDs for two main reasons: (i) the actual exciton binding energy in experiments is smaller than for an isolated 2D

DOI: 10.1021/acs.nanolett.7b03429
Nano Lett. 2017, 17, 6435−6442

system because of the additional screening provided by the substrate;[32,60−63] (ii) the intralayer exciton in single layer TMD decays into a charge-transfer exciton, where the carriers still experience the Coulomb interaction, rather than dissociating into a free electron and hole.[5,34,54,64] The barrier for decay from an intralayer to an interlayer exciton must be smaller than the binding energy of the intralayer exciton.

What is clear from our study is that the intrinsic phonon-assisted charge transfer mechanism is important for different TMD vdW heterojunctions since many of them have similar band structures and alignments. The details of the e−p coupling, however, would depend on the atomic masses and other material-dependent factors, which might affect phonon-assisted charge separation, but these factors can be addressed by straightforward application of the *ab initio* NAMD simulations. We expect that our atomic level perspective of the ultrafast charge transfer at the vdW heterostructure interface provides essential insights into the design and function of novel 2D devices for optoelectronic and photovoltaic applications.

■ ASSOCIATED CONTENT

Supporting Information

The Supporting Information is available free of charge on the ACS Publications website at DOI: 10.1021/acs.nanolett.7b03429.

NAMD calculations details including the K-point sampling, influence of the self-interaction error, FT transform of the Kohn−Sham eigenvalues, orbital spatial distribution at $WS_2\Sigma$, and vdW interaction effects of different stackings and various temperatures (PDF)

■ AUTHOR INFORMATION

Corresponding Author

*E-mail: zhaojin@ustc.edu.cn.

ORCID

Wissam A. Saidi: 0000-0001-6714-4832
Yu Xie: 0000-0001-8925-6958
Oleg V. Prezhdo: 0000-0002-5140-7500
Hrvoje Petek: 0000-0001-9605-2590
Jin Zhao: 0000-0003-1346-5280

Notes

The authors declare no competing financial interest.

■ ACKNOWLEDGMENTS

This work is supported by NSFC (11620101003, 21373190, 21421063, 91421313, 91233106, 21503248, and 21673266), by National Key R&D Program of China (2016YFA0200604, 2017YFA0204904), the Fundamental Research Funds for the Central Universities WK3510000005, and NSF DMR-1311845 grant. W.A.S. acknowledges a startup fund from the University of Pittsburgh. Z.L. acknowledges the Natural Science Foundation of Shandong Province for Distinguished Young Scholars (JQ201504). O.V.P. acknowledges financial support of the U.S. National Science Foundation, Grant No. CHE-1565704. Calculations were performed at Environmental Molecular Sciences Laboratory at the PNNL, a user facility sponsored by the DOE Office of Biological and Environmental Research and Argonne Leadship Computing Facility, which is a DOE Office of Science User Facility supported under Contract DE-AC02-06CHI1357 and USTC supercomputing center. We thank Z. Zhang and J. Yang for valuable discussions.

■ REFERENCES

(1) Geim, A. K.; Grigorieva, I. V. *Nature* **2013**, *499* (7459), 419−425.
(2) Georgiou, T.; Jalil, R.; Belle, B. D.; Britnell, L.; Gorbachev, R. V.; Morozov, S. V.; Kim, Y.-J.; Gholinia, A.; Haigh, S. J.; Makarovsky, O.; Eaves, L.; Ponomarenko, L. A.; Geim, A. K.; Novoselov, K. S.; Mishchenko, A. *Nat. Nanotechnol.* **2012**, *8* (2), 100−103.
(3) Hunt, B.; Sanchez-Yamagishi, J. D.; Young, A. F.; Yankowitz, M.; LeRoy, B. J.; Watanabe, K.; Taniguchi, T.; Moon, P.; Koshino, M.; Jarillo-Herrero, P.; Ashoori, R. C. *Science* **2013**, *340* (6139), 1427−1430.
(4) Ponomarenko, L. A.; Gorbachev, R. V.; Yu, G. L.; Elias, D. C.; Jalil, R.; Patel, A. A.; Mishchenko, A.; Mayorov, A. S.; Woods, C. R.; Wallbank, J. R.; Mucha-Kruczynski, M.; Piot, B. A.; Potemski, M.; Grigorieva, I. V.; Novoselov, K. S.; Guinea, F.; Fal'ko, V. I.; Geim, A. K. *Nature* **2013**, *497* (7451), 594−597.
(5) Hong, X.; Kim, J.; Shi, S.-F.; Zhang, Y.; Jin, C.; Sun, Y.; Tongay, S.; Wu, J.; Zhang, Y.; Wang, F. *Nat. Nanotechnol.* **2014**, *9* (9), 682−686.
(6) Lee, C. H.; Lee, G. H.; van der Zande, A. M.; Chen, W. C.; Li, Y. L.; Han, M. Y.; Cui, X.; Arefe, G.; Nuckolls, C.; Heinz, T. F.; Guo, J.; Hone, J.; Kim, P. *Nat. Nanotechnol.* **2014**, *9* (9), 676−681.
(7) Jones, A. M.; Yu, H.; Ross, J. S.; Klement, P.; Ghimire, N. J.; Yan, J.; Mandrus, D. G.; Yao, W.; Xu, X. *Nat. Phys.* **2014**, *10* (2), 130−134.
(8) Dai, S.; Fei, Z.; Ma, Q.; Rodin, A. S.; Wagner, M.; McLeod, A. S.; Liu, M. K.; Gannett, W.; Regan, W.; Watanabe, K.; Taniguchi, T.; Thiemens, M.; Dominguez, G.; Castro Neto, A. H.; Zettl, A.; Keilmann, F.; Jarillo-Herrero, P.; Fogler, M. M.; Basov, D. N. *Science* **2014**, *343* (6175), 1125−1129.
(9) Woessner, A.; Lundeberg, M. B.; Gao, Y.; Principi, A.; Alonso-Gonzalez, P.; Carrega, M.; Watanabe, K.; Taniguchi, T.; Vignale, G.; Polini, M.; Hone, J.; Hillenbrand, R.; Koppens, F. H. L. *Nat. Mater.* **2014**, *14* (4), 421−425.
(10) Withers, F.; Del Pozo-Zamudio, O.; Mishchenko, A.; Rooney, A. P.; Gholinia, A.; Watanabe, K.; Taniguchi, T.; Haigh, S. J.; Geim, A. K.; Tartakovskii, A. I.; Novoselov, K. S. *Nat. Mater.* **2015**, *14* (3), 301−306.
(11) Mishchenko, A.; Tu, J. S.; Cao, Y.; Gorbachev, R. V.; Wallbank, J. R.; Greenaway, M. T.; Morozov, V. E.; Morozov, S. V.; Zhu, M. J.; Wong, S. L.; Withers, F.; Woods, C. R.; Kim, Y. J.; Watanabe, K.; Taniguchi, T.; Vdovin, E. E.; Makarovsky, O.; Fromhold, T. M.; Fal'ko, V. I.; Geim, A. K.; Eaves, L.; Novoselov, K. S. *Nat. Nanotechnol.* **2014**, *9* (10), 808−813.
(12) Ju, L.; Velasco, J., Jr.; Huang, E.; Kahn, S.; Nosiglia, C.; Tsai, H.-Z.; Yang, W.; Taniguchi, T.; Watanabe, K.; Zhang, Y.; Zhang, G.; Crommie, M.; Zettl, A.; Wang, F. *Nat. Nanotechnol.* **2014**, *9* (5), 348−52.
(13) Padilha, J. E.; Fazzio, A.; da Silva, A. J. R. *Phys. Rev. Lett.* **2015**, *114* (6), 066803.
(14) Wang, X.; Xia, F. *Nat. Mater.* **2015**, *14* (3), 264−265.
(15) Britnell, L.; Ribeiro, R. M.; Eckmann, A.; Jalil, R.; Belle, B. D.; Mishchenko, A.; Kim, Y. J.; Gorbachev, R. V.; Georgiou, T.; Morozov, S. V.; Grigorenko, A. N.; Geim, A. K.; Casiraghi, C.; Castro Neto, A. H.; Novoselov, K. S. *Science* **2013**, *340* (6138), 1311−1314.
(16) Yu, W. J.; Liu, Y.; Zhou, H. L.; Yin, A. X.; Li, Z.; Huang, Y.; Duan, X. F. *Nat. Nanotechnol.* **2013**, *8* (12), 952−958.
(17) Wang, Q. H.; Kalantar-Zadeh, K.; Kis, A.; Coleman, J. N.; Strano, M. S. *Nat. Nanotechnol.* **2012**, *7* (11), 699−712.
(18) Feng, J.; Qian, X.; Huang, C.-W.; Li, J. *Nat. Photonics* **2012**, *6* (12), 865−871.
(19) Mak, K. F.; He, K. L.; Shan, J.; Heinz, T. F. *Nat. Nanotechnol.* **2012**, *7* (8), 494−498.
(20) Eda, G.; Yamaguchi, H.; Voiry, D.; Fujita, T.; Chen, M.; Chhowalla, M. *Nano Lett.* **2011**, *11* (12), 5111−5116.
(21) Mak, K. F.; Lee, C.; Hone, J.; Shan, J.; Heinz, T. F. *Phys. Rev. Lett.* **2010**, *105* (13), 136805−136805.
(22) Cheiwchanchamnangij, T.; Lambrecht, W. R. L. *Phys. Rev. B: Condens. Matter Mater. Phys.* **2012**, *85* (20), 205302.
(23) Ramasubramaniam, A. *Phys. Rev. B: Condens. Matter Mater. Phys.* **2012**, *86* (11), 115409.

(24) Bernardi, M.; Palummo, M.; Grossman, J. C. *Nano Lett.* **2013**, *13* (8), 3664−3670.
(25) Kang, J.; Tongay, S.; Zhou, J.; Li, J.; Wu, J. *Appl. Phys. Lett.* **2013**, *102* (1), 012111.
(26) Gong, C.; Zhang, H.; Wang, W.; Colombo, L.; Wallace, R. M.; Cho, K. *Appl. Phys. Lett.* **2013**, *103* (5), 053513.
(27) Komsa, H.-P.; Krasheninnikov, A. V. *Phys. Rev. B: Condens. Matter Mater. Phys.* **2013**, *88* (8), 085318.
(28) Terrones, H.; Lopez-Urias, F.; Terrones, M. *Sci. Rep.* **2013**, *3*, 1549.
(29) Kosmider, K.; Fernandez-Rossier, J. *Phys. Rev. B: Condens. Matter Mater. Phys.* **2013**, *87* (7), 075451.
(30) Qiu, D. Y.; da Jornada, F. H.; Louie, S. G. *Phys. Rev. Lett.* **2013**, *111* (21), 216805−216805.
(31) Jones, A. M.; Yu, H.; Ghimire, N. J.; Wu, S.; Aivazian, G.; Ross, J. S.; Zhao, B.; Yan, J.; Mandrus, D. G.; Xiao, D.; Yao, W.; Xu, X. *Nat. Nanotechnol.* **2013**, *8* (9), 634−638.
(32) Ugeda, M. M.; Bradley, A. J.; Shi, S.-F.; da Jornada, F. H.; Zhang, Y.; Qiu, D. Y.; Ruan, W.; Mo, S.-K.; Hussain, Z.; Shen, Z.-X.; Wang, F.; Louie, S. G.; Crommie, M. F. *Nat. Mater.* **2014**, *13* (12), 1091−1095.
(33) Ceballos, F.; Bellus, M. Z.; Chiu, H.-Y.; Zhao, H. *ACS Nano* **2014**, *8* (12), 12717−12724.
(34) Zhu, X. Y.; Monahan, N. R.; Gong, Z. Z.; Zhu, H. M.; Williams, K. W.; Nelson, C. A. *J. Am. Chem. Soc.* **2015**, *137* (26), 8313−8320.
(35) Stroppa, A.; Kresse, G. *New J. Phys.* **2008**, *6*, 063020.
(36) Kresse, G.; Hafner, J. *Phys. Rev. B: Condens. Matter Mater. Phys.* **1993**, *48*, 13115.
(37) Kresse, G.; Hafner, J. *Phys. Rev. B: Condens. Matter Mater. Phys.* **1994**, *49* (20), 14251−14269.
(38) Akimov, A. V.; Prezhdo, O. V. *J. Chem. Theory Comput.* **2014**, *10* (2), 789−804.
(39) Akimov, A. V.; Prezhdo, O. V. *J. Chem. Theory Comput.* **2013**, *9* (11), 4959−4972.
(40) Perdew, J. P.; Burke, K.; Ernzerhof, M. *Phys. Rev. Lett.* **1996**, *77*, 3865−3868.
(41) Blöchl, P. E. *Phys. Rev. B: Condens. Matter Mater. Phys.* **1994**, *50* (24), 17953.
(42) Grimme, G. *J. Comput. Chem.* **2006**, *27*, 1787.
(43) Nie, Z.; Long, R.; Sun, L.; Huang, C.-C.; Zhang, J.; Xiong, Q.; Hewak, D. W.; Shen, Z.; Prezhdo, O. V.; Loh, Z.-H. *ACS Nano* **2014**, *8* (10), 10931−10940.
(44) Duncan, W. R.; Prezhdo, O. V. *Annu. Rev. Phys. Chem.* **2007**, *58* (1), 143−184.
(45) Fischer, S. A.; Duncan, W. R.; Prezhdo, O. V. *J. Am. Chem. Soc.* **2009**, *131* (42), 15483−15491.
(46) Mai, C.; Semenov, Y. G.; Barrette, A.; Yu, Y.; Jin, Z.; Cao, L.; Kim, K. W.; Gundogdu, K. *Phys. Rev. B: Condens. Matter Mater. Phys.* **2014**, *90* (4), 041414.
(47) Mai, C.; Barrette, A.; Yu, Y.; Semenov, Y. G.; Kim, K. W.; Cao, L.; Gundogdu, K. *Nano Lett.* **2014**, *14* (1), 202−206.
(48) Dal Conte, S.; Bottegoni, F.; Pogna, E. A. A.; De Fazio, D.; Ambrogio, S.; Bargigia, I.; D'Andrea, C.; Lombardo, A.; Bruna, M.; Ciccacci, F.; Ferrari, A. C.; Cerullo, G.; Finazzi, M. *Phys. Rev. B: Condens. Matter Mater. Phys.* **2015**, *92* (23), 235425.
(49) Zhu, C. R.; Zhang, K.; Glazov, M.; Urbaszek, B.; Amand, T.; Ji, Z. W.; Liu, B. L.; Marie, X. *Phys. Rev. B: Condens. Matter Mater. Phys.* **2014**, *90* (16), 161302.
(50) Wu, F.; Qu, F.; MacDonald, A. H. *Phys. Rev. B: Condens. Matter Mater. Phys.* **2015**, *91* (7), 75310−75310.
(51) Zhao, Y.; Luo, X.; Li, H.; Zhang, J.; Araujo, P. T.; Gan, C. K.; Wu, J.; Zhang, H.; Quek, S. Y.; Dresselhaus, M. S.; Xiong, Q. *Nano Lett.* **2013**, *13* (3), 1007−1015.
(52) Molina-Sanchez, A.; Wirtz, L. *Phys. Rev. B: Condens. Matter Mater. Phys.* **2011**, *84*, 155413.
(53) Lui, C. H.; Ye, Z.; Ji, C.; Chiu, K.-C.; Chou, C.-T.; Andersen, T. I.; Means-Shively, C.; Anderson, H.; Wu, J.-M.; Kidd, T.; Lee, Y.-H.; He, R. *Phys. Rev. B: Condens. Matter Mater. Phys.* **2015**, *91* (16), 165403.
(54) Rivera, P.; Schaibley, J. R.; Jones, A. M.; Ross, J. S.; Wu, S.; Aivazian, G.; Klement, P.; Seyler, K.; Clark, G.; Ghimire, N. J.; Yan, J.; Mandrus, D. G.; Yao, W.; Xu, X. *Nat. Commun.* **2015**, *6*, 6242.
(55) Long, R.; Prezhdo, O. V. *Nano Lett.* **2016**, *16*, 1996−2003.
(56) Wang, H.; Bang, J.; Sun, Y.; Liang, L.; West, D.; Meunier, W.; Zhang, S. *Nat. Commun.* **2016**, *7*, 11504.
(57) Barbatti, M. *Wiley Interdiscip. Rev. Comput. Mol. Sci.* **2011**, *1*, 620−633.
(58) Parandekar, P. V.; Tully, J. C. *J. Chem. Phys.* **2005**, *122* (9), 094102.
(59) Parandekar, P. V.; Tully, J. C. *J. Chem. Theory Comput.* **2006**, *2* (2), 229−235.
(60) Cheiwchanchamnangij, T.; Lambrecht, W. R. L. *Phys. Rev. B: Condens. Matter Mater. Phys.* **2012**, *85*, 205302.
(61) He, J.; Hummer, K.; Franchini, C. *Phys. Rev. B: Condens. Matter Mater. Phys.* **2014**, *89*, 075409.
(62) Kylanpaa, I.; Komsa, H.-P. *Phys. Rev. B: Condens. Matter Mater. Phys.* **2015**, *92*, 205418.
(63) Komsa, H.-P.; Krasheninnikov, A. V. *Phys. Rev. B: Condens. Matter Mater. Phys.* **2012**, *86*, 241201.
(64) Yu, Y. F.; Hu, S.; Su, L. Q.; Huang, L. J.; Liu, Y.; Jin, Z. H.; Purezky, A. A.; Geohegan, D. B.; Kim, K. W.; Zhang, Y.; Cao, L. Y. *Nano Lett.* **2015**, *15* (1), 486−491.

DOI: 10.1021/acs.nanolett.7b03429
Nano Lett. 2017, 17, 6435−6442